Silicon (2024) 16:4437–4449
https://doi.org/10.1007/s12633-024-03012-w

RESEARCH

Characterization of Al-Si Alloy Reinforced with B_4C and TiO_2 Nanoparticles

P. K. Dinesh Kumar[1] · S. Darius Gnanaraj[1]

Received: 19 December 2023 / Accepted: 28 April 2024 / Published online: 9 May 2024

Abstract

Al-Si alloy as a matrix in Aluminium Metal Matrix Composites (AMCs) augments the hardness and strength. The work reports the characterization and mechanical properties of Hybrid Aluminium Metal Matrix Nanocomposites (HAMNCs) using Hypereutectic Al-Si grade LM30 alloy as the matrix with boron Carbide (nB_4C) and Rutile ($nTiO_2$) nanoparticles as reinforcements. Liquid metallurgy route ultrasonic squeeze-assisted stir-casting was employed to manufacture hybrid formulations. The HAMNC specimens were fabricated by maintaining 1 wt.% of nB_4C and by varying TiO_2 nanoparticles in steps of 0.25 wt.% in the 0 to 1 wt.% range. The optical micrographs revealed that ultrasonic vibration and squeeze casting effects aided the uniform distribution of nano reinforcements and lowered the porosity. XRD analysis revealed the formation of Aluminum Titanium Silicate ($Al_4Ti_2SiO_{12}$) due to the addition of $nTiO_2$. The results highlighted that the LM30 matrix having 1.0 wt.% of nB_4C and 0.75 wt.% of $nTiO_2$ exhibited the maximum hardness of 107.2 HRB, ultimate tensile strength of 265.52 MPa, and compressive strength of 656 MPa. The tensile fractography using FESEM highlighted the various kinds of dendrites associated with the fracture. nB_4C and TiO_2 nano reinforcements increased energy absorption during impact failure.

Keywords Ultrasonic · Stir-Casting · Electron Microscopy · X-ray Diffraction · Mechanical properties

1 Introduction

The adoption of Metal Matrix Composites (MMCs) has become more prevalent in numerous automotive applications due to their superior specific modulus, strength, ease of manufacturing, cost-effectiveness, and exceptional resistance to wear [1]. Because of their lightweight, excellent mechanical qualities, and wear-resistant behavior, aluminum matrix composites (AMCs) are one of the most essential MMCs in the transportation industry [2].

To attain excellent mechanical and tribological properties, hypereutectic Al-Si alloys with near eutectic composition (silicon more than 12.8 wt.%) are a promising option for automotive components such as brake rotors, pistons, and cylinder heads [3]. Also, the presence of Si in these alloys possesses characteristics such as greater flowability, improved castability leading to fewer casting flaws, and capacity to form intermetallic compounds [4]. The Hypereutectic Al-Si alloys comprise a proeutectic silicon (Si) phase and an Al-Si eutectic phase combination. The primary silicon particles in hypereutectic alloys pose higher hardness than α-aluminum, which acts like a load-bearing element compared with hypoeutectic Al-Si alloys. Including hard ceramic reinforcement followed by mechanical stirring of the alloy enhances the distribution of proeutectic silicon during casting. The most cost-effective way to improve the mechanical characteristics of these alloys is to strengthen them with ceramic materials. Ceramic materials have excellent interfacial interaction with the aluminium matrix [5].

Several researchers revealed that AMCs with Al-Si alloy as a parent matrix are best suited for pistons, brake rotors, and drums due to their superior strength and toughness [6]. Typically, AMCs are manufactured by encapsulating synthetic ceramics such as SiO_2, Al_2O_3, TiO_2, ZrO_2, h-BN, SiN, SiC, TiC, and B_4C as reinforcements [7].

Jayaprakash et al. [8] studied the mechanical properties of Al-Si alloy LM25 reinforced with SiC/Gr Particles through a double stir-casting process. They reported that the hybrid nanocomposite containing 4 wt.% SiC + 2 wt.% Gr exhibited increased tensile strength, yield Stress, elongation percentage, and hardness. Rajeev et al. [9] evaluated

✉ S. Darius Gnanaraj
dariusgnanaraj.s@vit.ac.in

1 School of Mechanical Engineering, Vellore Institute of Technology, Vellore 632104, India

the mechanical and tribological behavior of three different Al-Si grade alloys such as A319, A336, and A390, reinforcing with 15 wt.% SiC. They concluded that A319 + 15 wt.% SiC provided better mechanical behavior than other composites. Gnaneswaran et al. [10] conducted Mechanical and Wear Behaviors of LM6 alloy reinforced with copper-coated short steel fiber (0, 2.5, 5, and 10 wt.%) and 5% B4C. They revealed that the tensile strength of LM6 alloy hybrid composites (5 wt. % short steel fiber + 5% B4C) increased and exhibited a decreasing trend beyond the 5 wt.% addition of steel fibers.

Stir casting, a liquid-state manufacturing method, offers advantages like enhanced matrix-particle bonding, uniform reinforcement distribution, and mass production. This traditional stir-casting employment in AMCs is limited to micro-sized ceramic particles due to the tendency to agglomeration in an aluminium matrix [11]. In recent years, aluminum metal matrix nanocomposites (AMNCs) made from synthetic nanoparticles (< 100 nm) have attracted a more attention than AMCs made from micro ceramics because of their superior strength, high modulus, load-bearing ability, and thermal properties. Further, the reduced size and morphology of the nanoparticle reinforcements improve the AMNC's rigidity and stability [12]. When employing conventional stir-casting to produce AMNCs, the higher surface area of nanoparticles makes them more likely to agglomerate, leading to irregular distribution and increased porosity. Using cavitation and acoustic streaming effects from the ultrasonic vibration (UV) unit, ultrasonic-assisted stir-casting guarantees high wettability and homogenous dispersion of nanoparticles in the aluminium matrix to address these limitations [13]. Additionally, limited research has shown that squeeze-casting attachment with ultrasonic-assisted stir-casting lowers microporosity and refines the nanocomposite microstructures [14]. The need for lightweight Hybrid Aluminum Metal Matrix Composites (HAMCs) is driven by their potential to revolutionize aerospace and automotive industries that demand materials with high strength-to-weight ratios. Recent research indicates that HAMCs outperform single reinforcements regarding mechanical strength and wear resistance. Hence, interest in using ultrasonic-squeeze-assisted stir-casting to develop HAMNCs while incorporating more than one nano reinforcement among researchers has grown widely.

Pragathi P et al. [15] made a comparative study on Al + nSiC + n-wastecatalyst manufactured by squeeze and ultrasonic squeeze stir-casting methods. They identified that the latter casting route significantly improved the microstructures and mechanical properties. Hariharan et al. [16] fabricated AA1030 + nB_4C + n-hBN through an ultrasonic stir-casting process. The results highlighted that the UV effect broke the nanoparticle clusters, and a 40% increase in ultimate tensile strength over monolithic Al material was achieved. Kannan et al. [17] developed the AA7075 + nAl_2O_3 + SiC by squeeze and stir casting methods. They found that squeeze-casted hybrid nanocomposites had low porosity and enhanced tensile strength. Shayan et al. [18] synthesized AA2024-$nTiO_2$ + $nSiO_2$ hybrid AMNC using a stir-casting process. The results indicated that the addition of nanoparticles reduced the grain size and improved the mechanical properties.

Boron carbide (B_4C), the third hardest element after diamond and CBN, excels as a reinforcement due to its high hardness, low density, mechanical strength, and wear resistance [19]. Dinesh Kumar P.K. et al. [20] studied the effect of nB_4C particles on LM30 alloy fabricated using an ultrasonic-squeeze-assisted stir-casting route. They reported that LM30 nanocomposites with a maximum inclusion of 1 wt.% nB_4C exhibited enhanced mechanical performances due to the modifications of primary Si in the Al-Si matrix. Rutile, a cost-effective form of TiO_2 with robust mechanical and thermal attributes, enhances load-bearing capacity [21]. Shayan et al. [22] developed AA2024-$nTiO_2$ nanocomposites using a stir-casting process and revealed a significant enhancement in mechanical properties due to adding $nTiO_2$. Limited research has been done to study the effects of dual nanoparticles as reinforcements and Al-Si alloy as a matrix. Literature reports that research work has yet to be carried out to find the effect of B_4C and TiO_2 nanoparticle reinforcements on the hypereutectic Al-Si grade alloy matrix. Hence, this research focuses on developing novel Hybrid Aluminum Metal Matrix Nanocomposites by adding nano-sized B_4C and TiO_2 particles to the LM30 matrix using an ultrasonic-squeeze-assisted stir casting technique. The casted HAMNCs were tested for density, XRD, hardness, impact energy, tensile, and compressive strengths. Microstructural analysis was carried out. The fractured tensile surfaces were analyzed using Field Emission Scanning Electron Microscopy (FESEM) to study the fracture features. Transmission Electron Microscope (TEM) was used to ensure the uniform distribution on nanoparticles in the LM30 matrix.

2 Materials, Manufacturing and Experimental Methods

The Al-Si grade LM30 matrix ingots were purchased from Vision Castings India, and their chemical composition was determined through optical emission spectrometry, shown in Table 1. B_4C and TiO_2 nanoparticles of average particle size 80 and 50 nm used as reinforcements were procured from Nanoshel, USA, and SRL Chemicals, India. Figure 1 shows the FESEM micrographs and Energy Dispersive Spectroscopy (EDS) analysis of the nanoparticles using FEI Quanta-250, Thermo Fisher, USA.

Table 1 LM 30 alloy chemical composition in wt.%

Elements	Si	Cu	Mg	Fe	Ti	Al
Wt. %	17.604	4.839	0.598	0.282	0.410	76.267

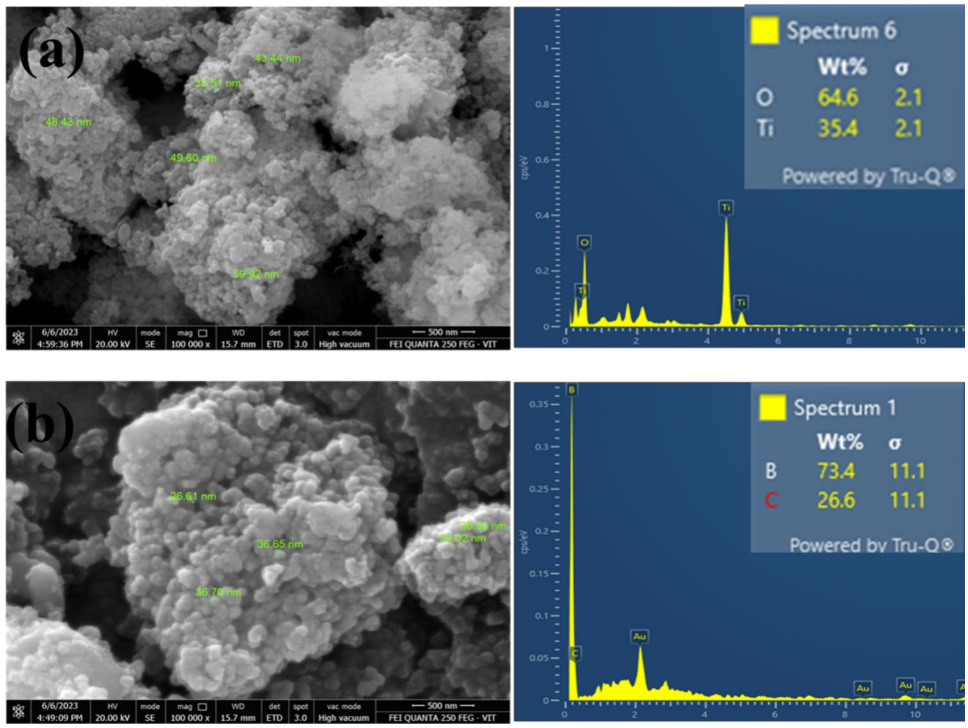

Fig. 1 FESEM with EDS analysis of (**a**) Rutile ($nTiO_2$) and (**b**) Boron Carbide (B_4C) nanoparticles

Figure 2 shows the experimental setup used for the manufacturing of hybrid nanocomposites. The LM30 alloy was preheated to 100 °C to remove moisture. At 800 °C, the ingots were melted for 60 min. Following it, 0.5 wt.% hexachloroethane tablets were added to degas hydrogen. Then, stirring was carried at 450 rpm for 10 min, 1% Mg ribbons were added for nanoparticle wettability. Afterwards, the stirring speed was reduced to 250 rpm, and 0.25 wt.% of $nTiO_2$ was added while keeping nB_4C at 1 wt. %. A similar procedure was carried out for fabricating specimens with 0.5wt.%, 0.75 wt.% and 1.0 wt.% of $nTiO_2$. An ultrasonic probe at 20 kHz created high-energy ultrasonic vibration (UV) waves to disperse cavitation bubbles and agglomerations in the liquid pool [23]. The composite was poured into a preheated cast iron mold, subjected to 150 MPa squeezing pressure, and cooled to solidify. The fabricated as-cast LM30 alloy and hybrid nanocomposites were labeled based on the weight percent of reinforcements on the base alloy and listed in Table 2.

Porosity affects the properties of cast products. Nanoparticles introduced cause porosity due to the ambient air they carry inside the molten pool. While porosity cannot be eliminated, it may be regulated during manufacturing. As per ASTM B962–13 standards, the porosity of the casted formulations was calculated. Mettler Toledo's density kit, ML-DNY-43, measured the mass of the base alloy and hybrid nanocomposites in air and water using Archimedes' principle to calculate the experimental density. The theoretical density was calculated using the rule of mixture, $\frac{100}{\rho_{theoretical}} = \left[\frac{matrix\ wt.\%}{\rho_{matrix}} + \frac{reinforcement\ wt.\%}{\rho_{reinforcement}}\right]$. The porosity percentage of the nanocomposites was then determined using the formula, $porosity = \left[\left(1 - \frac{\rho_{experimental}}{\rho_{theoretical}}\right)100\right]$.

The reinforced hybrid nanocomposite specimens and the LM30 alloy were polished per accepted metallographic practices. Then, samples were etched using Keller's reagent, and microstructures were examined using an optical microscope (OM). The materials were further subjected to metallographic testing with a FESEM equipped with an EDS (Make-FEI Qunata-250, Thermo Fisher, USA) to identify the elemental compounds in the nanocomposites. Further, the distribution of nanoparticles and microstructure of the processed hybrid nanocomposites was performed using (Make- JEOL TEM, JEM -F200). The LM30 hybrid nanocomposites were examined using the Bruker X-Ray Diffraction Model to conduct compound analysis and detect the presence of base alloy and reinforced

Fig. 2 Squeeze-assisted stir-casting experimental setup with UV supplement used in the study

Table 2 Identifications of hybrid nanocomposites fabricated in the present study

No	Notations used	LM30 (Wt. %)	nB_4C (Wt. %)	$nTiO_2$
1	H0	100	-	-
2	H1	99	1	-
3	H2	98.5	1	0.25
4	H3	98.0	1	0.50
5	H4	97.5	1	0.75
6	H5	97.0	1	1

particle elements. The radiation range was applied between 5°-90°, and the radiation source was Cu-Kα.

LM30 base alloy and hybrid nanocomposites were tested for resistance to indentation using a Rockwell hardness tester on a 'B' scale under a load of 100 kgf. Also, the values for hardness represented are the average of 5 measurements for a particular composition. The tensile tests were conducted on the base metal and hybrid nanocomposites by ASTM E8 standard. The INSTRON 8801 Universal Testing Machine (UTM) was used at a 0.5 mm/min rate to measure the Ultimate Tensile Strength (UTS) and elongation percentage. The HAMNC's compressive strength was assessed following the ASTM E9 standard, with a fixed feed rate of 2 mm/min and employing a (L/D) ratio of 2. Afterwards, the hybrid nanocomposite impact resistance was tested using a Charpy V-notch test for high strain rates. The testing procedure followed the ASTM E-23 standard. Figure 3 shows the schematic of the prepared samples machined to evaluate various mechanical properties based on the standards using a wire-cut Electric Discharge Machine (EDM) facility from the cast products. The assessment was repeated three times for each formulation, and the average results were reported.

3 Results and Discussions

3.1 Microstructure Examination

The optical micrographs of the reinforced hybrid nanocomposite specimens and the LM30 alloy are shown in Fig. 4. The hypereutectic LM30 alloy is made of Al-Si and primary silicon eutectic phases. LM30 alloy optical micrographs Fig. 4(a) shows a coarse polyhedral structure (primary Si phase) in a eutectic matrix. The alloy's primary silicon solidifies into faceted structures before transitioning to eutectic solidification. Since the alloy contains polyhedral-shaped primary silicon, it classifies to be hypereutectic. Due to the UV effect, eutectic silicon had equally disseminated and encircled the reinforced nanoparticles (Fig. 4(b-d)). Additionally, within the nanocomposites, the primary silicon morphology underwent refinement, transitioning from a coarser size to a finer size, and became more evenly distributed compared to the base alloy. Compared with Fig. 4(a), it is clearly shown from Fig. 4(c-f) that the addition of nanoceramics reinforcement demonstrated the decrease in the size of the eutectic silicon grain. Mismatches in heat conductivity and changes in the density of strengthened nanoparticles were found to cause changes in metallographic structures [24]. Also, the solidification process under squeeze-pressure raised the liquidus temperature of LM30 alloy, which led to a significant undercooling of the melt. Furthermore, the application of pressure eliminated the creation of air gaps between the melt and the die, resulting in a significant improvement in the cooling efficiency and heat transfer coefficient. The formation of a fine-grained microstructure was aided by a faster cooling rate [25].

The main Si phase and homogeneous distribution of nano reinforcements inside the LM30 matrix were revealed by the FESEM with Energy Dispersive Spectroscopy (EDS) investigation. The EDS intensity peaks in Fig. 5 showed the primary elements, such as Al, Si, Cu, and Mg, corresponding to the base material. Additionally, nanoparticles employed as reinforcement were indicated by the B, C, Ti, and O elemental spectrums. Further, the uniform dispersion of nanoparticles and primary Si phase was detected using TEM as depicted in Fig. 6.

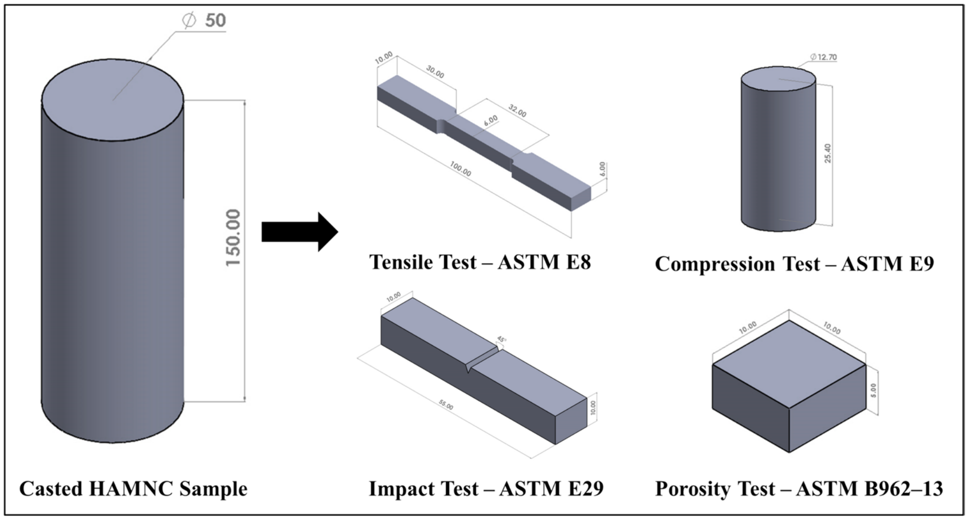

Fig. 3 Schematic view of as-cast HAMNC and its associated mechanical study samples as per ASTM standards

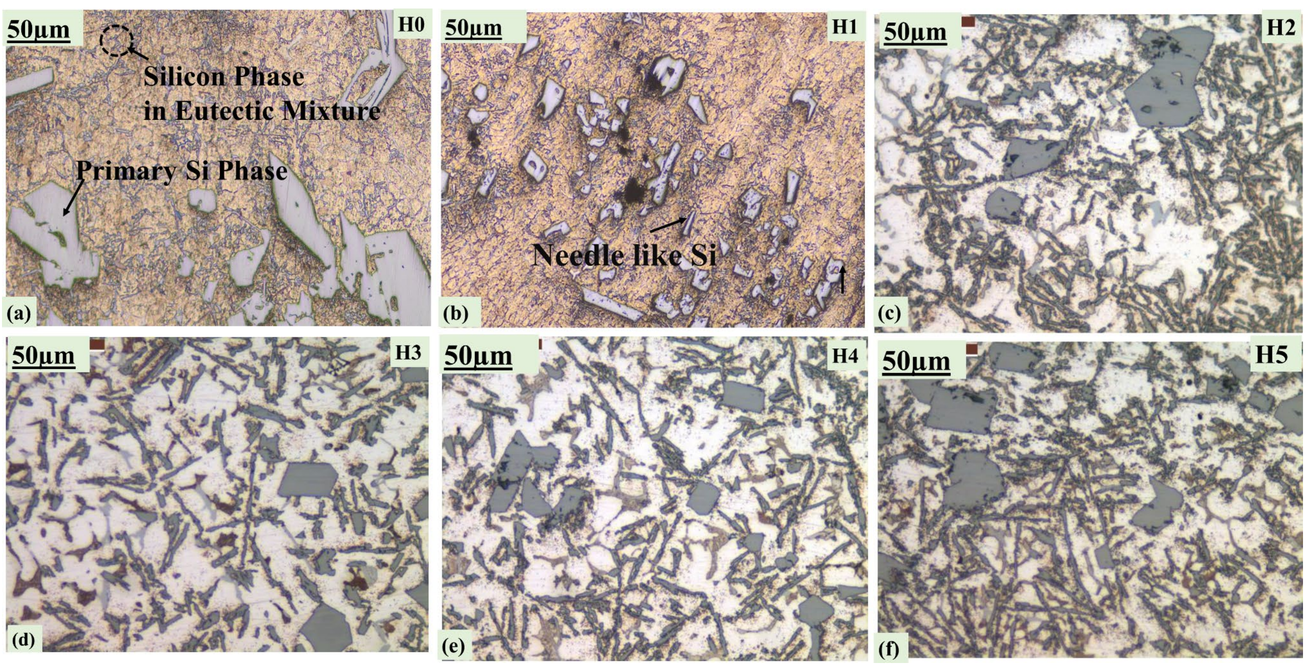

Fig. 4 **a**–**f** Microstructure of LM30 + nB_4C + $nTiO_2$ hybrid nanocomposites using Optical Microscopy

3.2 XRD Elemental Analysis

In the case of HAMNCs, the XRD spectrum peaks witnessed in Fig. 7 were identified by JCPDS numbers. Several additional peaks were observed, suggesting the existence of interfacial reaction products, the presence of reinforced particles, and the formation of intermetallic compounds. The JCPDS and corresponding elements were listed as Aluminum (03–065-2869), Silicon (01–089-9054), Aluminum Silicon (00–041-1222), Aluminum Copper (00–025-0012), Magnesium Silicon (01–073-2246), and Aluminum Copper Magnesium (01–074-5175) which are indicative of the monolithic LM30 base material with intermetallic compounds. Subsequent XRD analysis of the H4 hybrid nanocomposite unveiled the development of a strengthening compound, Aluminum Titanium Silicate (00–045-1206), resulting from incorporating $nTiO_2$. The occurrence of interfacial reaction on reinforced particles has been demonstrated to result in better wetting behavior. Hence, the presence of stronger interfacial bonding in hybrid nanocomposites may be attributed to the formation of the interfacial compound ($Al_4Ti_2SiO_{12}$) on $nTiO_2$ addition [26]. An interfacial reaction

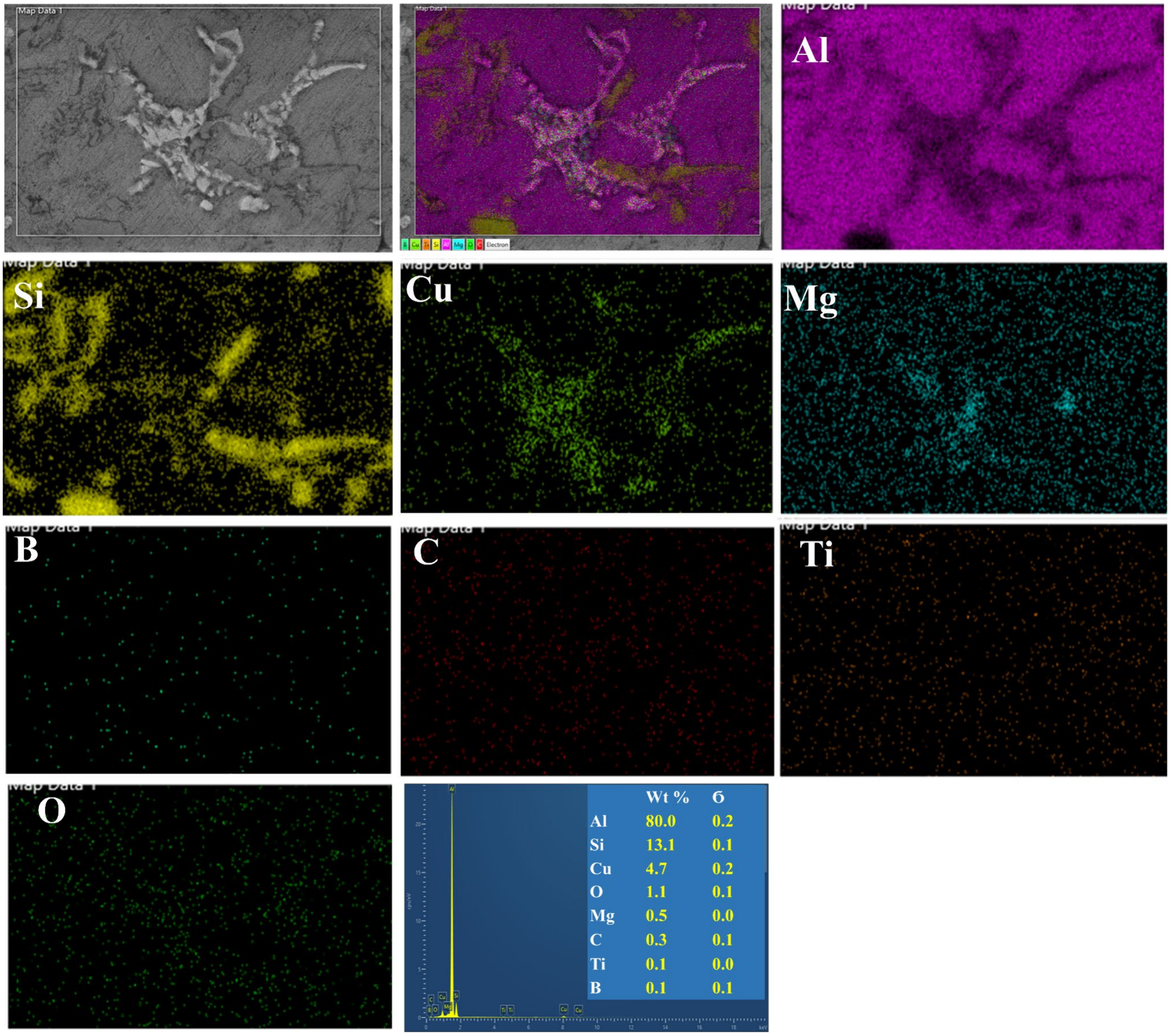

Fig. 5 FE-SEM and EDS analysis of TiO_2 reinforced LM30 + 1 wt. nB_4C hybrid nanocomposite

of this kind did not occur when only B_4C nanoparticles were added. Furthermore, the XRD intensity peak verified the existence of B_4C (00–001-1163) and TiO_2 (00–015-0875) nanoparticles.

3.3 Density and Porosity Evaluation

Figure 8 shows the comparison of theoretical and experimental densities with the porosity percent of the HAMNCs. Theoretical and experimental density values of LM30 alloy and its hybrid nanocomposites exhibited a comparable trend and were closely aligned with each other. From the graph, it is evident that, the theoretical density increased with the addition of reinforcement contents. Up to 0.75 wt.% addition of $nTiO_2$ particles to the LM30/nB_4C mixture, the experimental density increased with the reduction in porosity percent.. Incorporating nanoparticle reinforcements at a lower weight percentage increased fluidity during casting. The enhanced fluidity facilitated the easy flow of the molten metal into the mold cavities, hence minimizing the occurrence of porosity in the hybrid nanocomposites. Nanoparticles served as the nucleation sites for the solidification of the LM30 alloy. Thus, the dual nano reinforcements facilitated the initiation of solidification by providing surfaces that promote the creation of finer and more evenly dispersed solid phases. It facilitated a more optimal arrangement of the solid phase during the process of solidification, hence minimizing the occurrence of voids and porosity [27]. Further, it is confirmed that the combined effects caused by UV treatment which helped in the proper distribution of

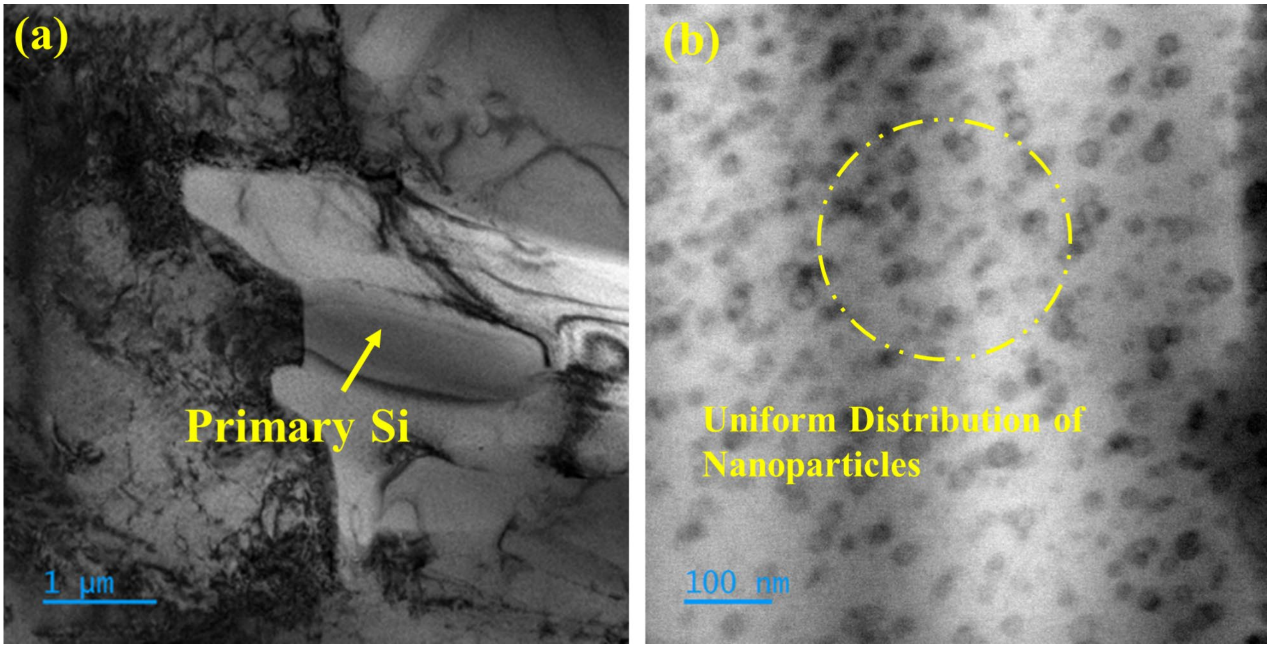

Fig. 6 Transmission Electron Micrograph of 0.75wt.% TiO_2 reinforced LM30 + 1 wt. nB_4C (**a**) 1µm marker and (**b**) 100nm marker

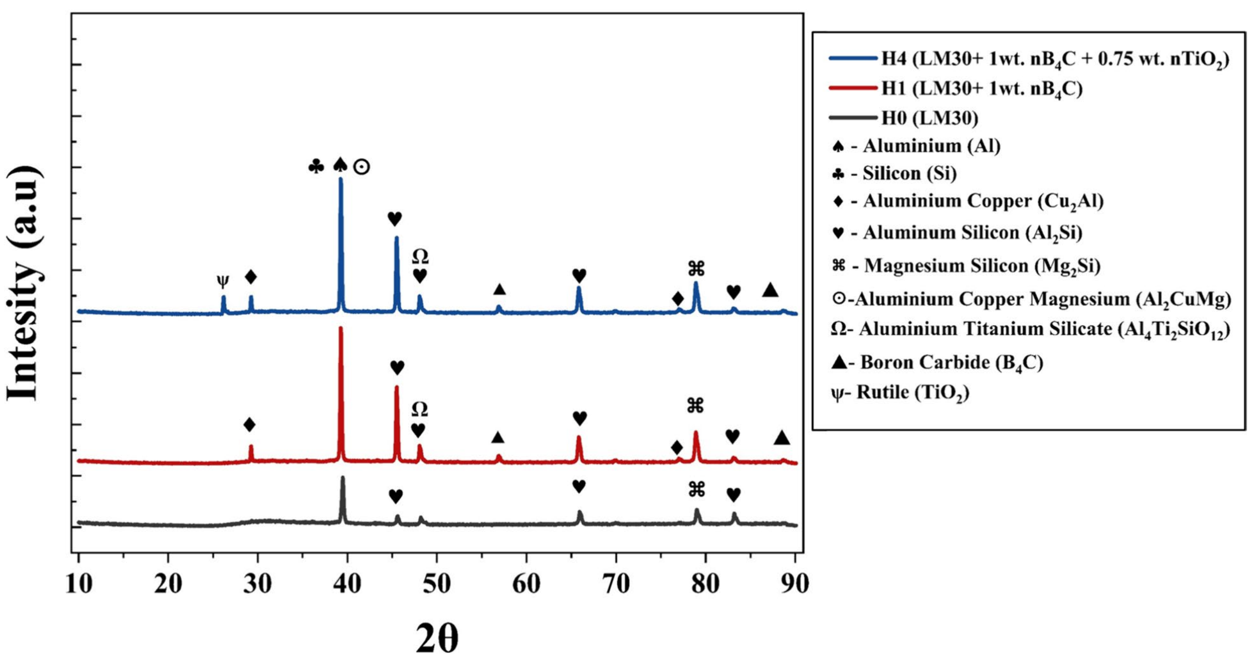

Fig. 7 XRD spectrum of LM30 alloy and hybrid nanocomposites

nanoparticles and the high squeeze pressure of 150 MPa during casting reduced porosity. The $nTiO_2$ particle density (4.23 g/cm^3) was higher than nB_4C (2.52 g/cm^3) and the LM30 matrix (2.77 g/cm^3) raised actual density. Because of the high surface area to volume ratio of the nanoparticles, porosity increases with an increase in the $nTiO_2$ reinforcement. Increased porosity results from developed clusters that acted as nucleation sites for void formation after the limit of reinforcement has been exceeded in the molten pool [28]. At increasing levels of nanoparticle addition, it became more difficult to achieve a uniform distribution of nanoparticles. Also, the difference in the thermal expansion coefficients between the molten matrix and nanoparticles (LM30 matrix –24 X 10^{-6} K^{-1}, B_4C – 5.76 X 10^{-6} $K^{-1}$and TiO_2 – 15.12 X

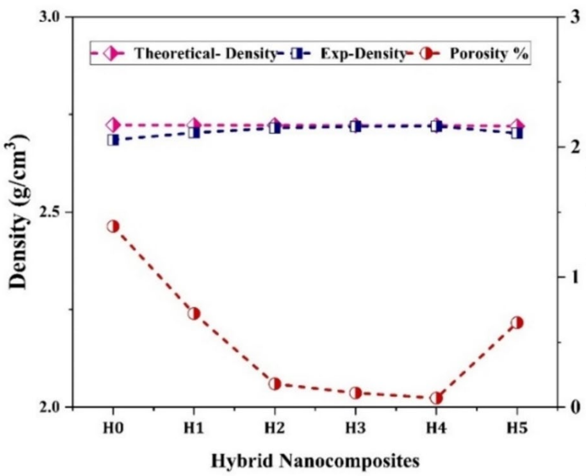

Fig. 8 Theoretical Vs Experimental Densities Vs Porosity graph of LM30 + nB_4C + $nTiO_2$ hybrid nanocomposites

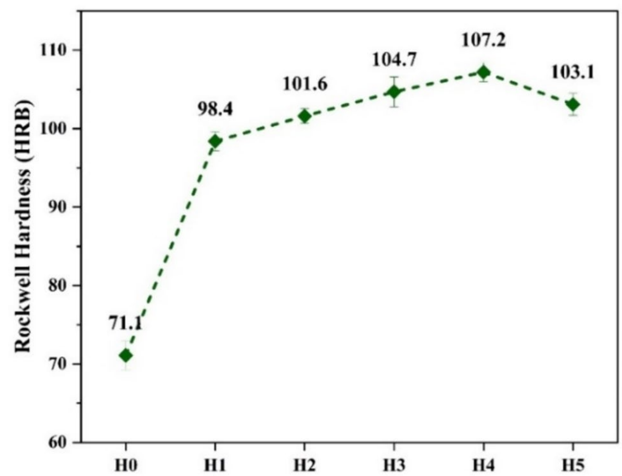

Fig. 9 Rockwell hardness of the LM30 alloy and hybrid nanocomposites

10^{-6} K^{-1}) might result in thermal stresses during solidification or cooling. Hence, the addition of $nTiO_2$ particles to the LM30 + 1 wt.% nB_4C formulation leads to void formation and increased porosity.

3.4 Mechanical Properties of HAMNCs

To understand individual reinforcement's role in hybrid nanocomposites' strengthening factor, the mechanical properties of LM30 alloy reinforced with nB_4C particles are illustrated in Table 3. The nanocomposite comprising LM30 alloy with 1 wt.% nB_4C, which performed better among other materials, is taken as the base, and the effect of reinforcing $nTiO_2$ with it is explored in this work.

3.4.1 Rockwell Hardness

The change in Rockwell hardness of cast LM30 alloy, LM30 + nB_4C, and (LM30 + nB_4C + $nTiO_2$) processed combinations is shown in Fig. 9. Adding $nTiO_2$ reinforcements to the LM30 + nB_4C matrix increased the bulk hardness. The maximum increment was exhibited by the H4 composite with 50.77% HRB compared to the monolithic LM30 alloy. The introduction of dual nano reinforcements made the hybrid nanocomposite matrix denser and more rigid. Further, incorporating rigid double ceramic particles and reduced inter-particle spacing effectively impeded the motion of dislocations in nanocomposites [8]. The compounds such as Al_2Si, Cu_2Al, Al_2CuMg, Mg_2Cu, and $Al_4Ti_2SiO_{12}$ confirmed from XRD results also increased the hardness. However, both the hardness values started to decline with the increase in $nTiO_2$ content due to the agglomerations that caused cavities during the fabrication process. Therefore, there is a consistent correlation between enhanced strength in hybrid AMNCs and reduced porosity.

3.4.2 Tensile Strength Evaluation

Figure 10(a) illustrates the HAMNC fractured tensile test specimens. The tensile strength variation of cast LM30 alloy and fabricated nanocomposites is shown in Fig. 11(a). The hybrid formulation samples demonstrated a noteworthy increase in UTS compared to the LM30 alloy and LM30 with 1 wt. % B_4C. The enhanced performance of UTS may

Table 3 Mechanical properties of LM30 alloy reinforced with nano B4C particles

No	Notations used	Rockwell Hardness (HRB)	Tensile Strength (MPa)	Elongation Percentage	Compression Strength (MPa)	Impact Strength (J)
1	LM30 alloy	71.1	148.56	0.51	479	6.4
2	LM30 + 0.5 wt. % nB_4C	86.7	176.46	0.62	530	8.2
3	LM30 + 1.0 wt. % nB_4C	98.4	211.5	0.83	612	10.3
4	LM30 + 1.5 wt. % nB_4C	91.2	185.05	0.76	586	9.5
5	LM30 + 2.0 wt. % nB_4C	88.3	159.77	0.61	496	8.4

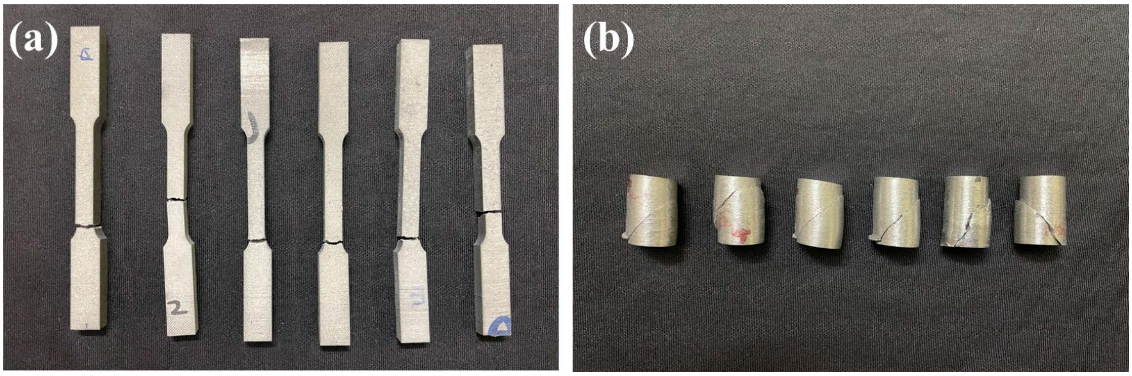

Fig. 10 Fractured nanocomposites (**a**) Tensile and (**b**) Compressive specimens

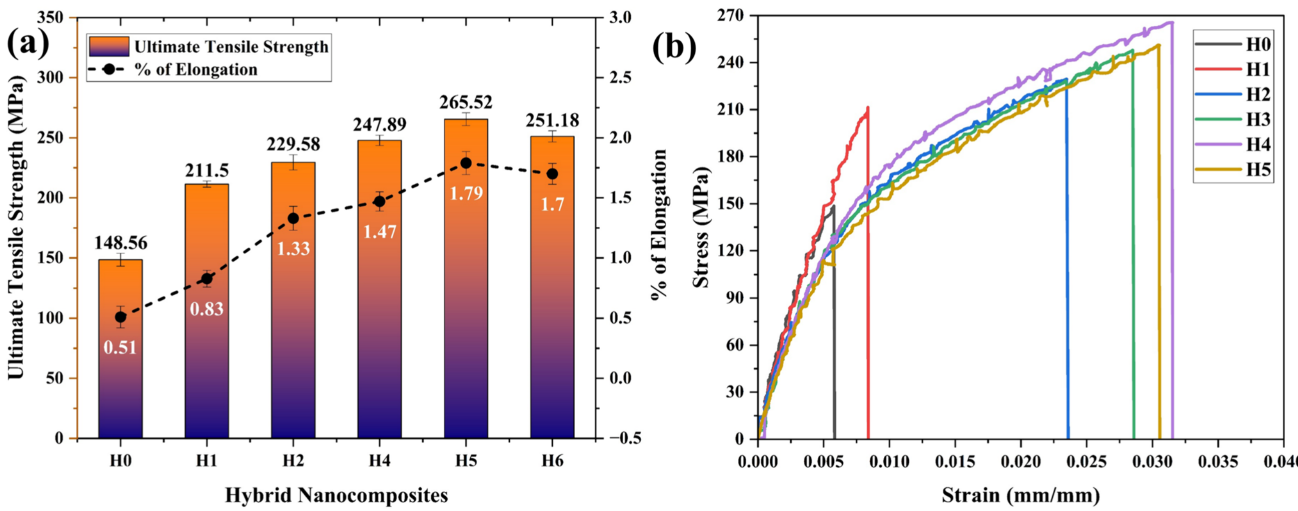

Fig. 11 LM30 + nB_4C + $nTiO_2$ hybrid nanocomposites (**a**) Ultimate Tensile Strength & Elongation Percentage, and (**b**) Tensile Stress Vs Strain

be ascribed to the integration of nB_4C and $nTiO_2$ nanoparticles as a means of reinforcement. This inclusion refines the proeutectic Si phase and limits dislocation mobility owing to the thermal mismatch between the alloy and dual nanoparticles, specifically the thermal conductivity (LM30 matrix—134 Wm^{-1} K^{-1}, B_4C -35 Wm^{-1} $K^{-1}$and TiO_2 – 4.8 Wm^{-1} K^{-1}) [4]. The observed increase in dislocation density had a crucial impact on enhancing the UTS of HAMNCs. The HAMNC's tensile strength has increased due to an enhanced load transmission mechanism between the LM30 matrix and nano reinforcements. When a tensile load was applied, the nB_4C and $nTiO_2$ reinforcement functioned as a barrier to the dislocation motion. The uniform dispersion of nanoparticles obtained by UV treatment prolonged the localized damage to the casted composites and assisted in the uniform stress distribution [29]. The inter-reaction compound $Al_4Ti_2SiO_{12}$ developed due to the $nTiO_2$ addition confirmed by XRD analysis has created transition layers that might have improved the interfacial bonding between the LM30 alloy. Specifically, the UTS of the hybrid nanocomposite containing 0.75 wt.% $nTiO_2$ showed a remarkable improvement of 78.73% over the virgin base alloy. Furthermore, the HAMNCs also noticed a similar trend, as shown in Fig. 11(b), in the proportion of elongation behavior. Due to the ultrasonic degassing effect, properly reinforced nanoparticle dispersion in the parent alloy matrix improved the stress distribution during deformation. Improved dispersion reduces stress concentrations, inhibits fracture formation and enhances material elongation. Also, the addition of dual reinforcements made the primary Si phase a finer grain structure (Fig. 4(b-f)) and helped plastic deformation. Hence, the material's ductility and elongation behavior increased. The H4 material exhibited the maximum elongation percentage at about 1.79%, whereas the base material could withstand 0.51%.

The tensile fracture morphologies of the LM30 base matrix, H1 (LM30 + 1 wt. nB_4C), optimally performed H4 (LM30 + 1 wt. nB_4C + 0.75wt. TiO_2), and maximum reinforcement H5 (LM30 + 1 wt. nB_4C + 1wt. TiO_2) were studied using FESEM are shown in Fig. 12. The fracture surface of the LM30 alloy matrix sample (Fig. 12a) displays considerable grape-shaped dendritic globules. Dendritic microstructure in B_4C reinforced nanocomposites (Fig. 12b) acts as a weak zone and stress riser, causing cracks. Micro holes caused by the alloy matrix and nanoparticle contact act as stress concentration points. Figure 12(c-d) shows the interfaces between the soft alloy matrix and stepwise dendritic ceramic nanoparticles that cause micro-holes [11]. The reduction in voids and micro-cracks is evident in the H4 composite compared to the base alloy and LM30 + 1%B_4C nanocomposite. Adding $nTiO_2$ reinforcement above 0.75 wt.% to the LM30 + 1wt.% nB_4C combination decreased ductility and made the hybrid nanocomposites more brittle due to the agglomeration of nanoparticles. This resulted in the accelerating failure of nanocomposite and reduced mechanical strength.

3.4.3 Compressive Strength Analysis

Figure 10(b) shows the HAMNC fractured compression test specimens. Figure 13 shows the Ultimate Compressive Strength (UCS) of the LM30 base material, LM30 + nB_4C nanocomposite, and $nTiO_2$-reinforced LM30 + nB_4C hybrid nanocomposites. The presence of more than 17 wt.% of Si in the matrix, which has higher hardness, played a vital role in the load-bearing ability of the casted HAMNCs. The merits of nano-size particles, attained due to the UV and squeezing pressure effects inside the soft LM30 matrix, enhanced the possibility of establishing a consistent distribution of reinforcement particles [30]. Consequently, this leads to an enhancement in Ultimate Compressive Strength (UCS) dislocation density. Additionally, the increased surface area-to-volume ratio of the nano reinforcements facilitated a more pronounced interaction between the LM30 matrix and the nanoparticles [29]. These characteristics enabled a strong connection among the matrix and dual nano reinforcements, resulting in a 36.95% increase in UCS by H4 compared to LM30 material. The rise in UCS may also be

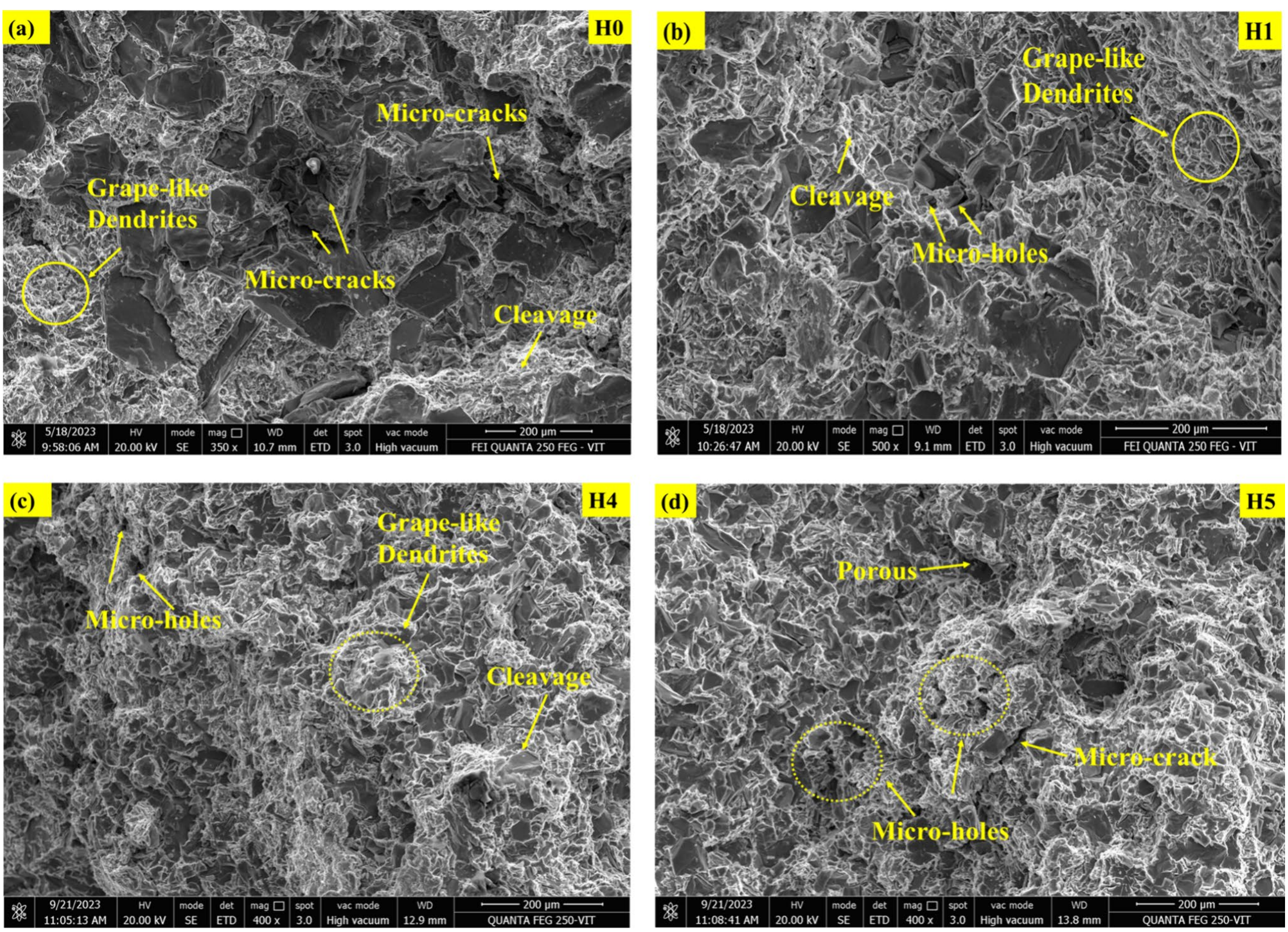

Fig. 12 **a-d** Tensile fracture morphologies of hybrid nanocomposites using FESEM

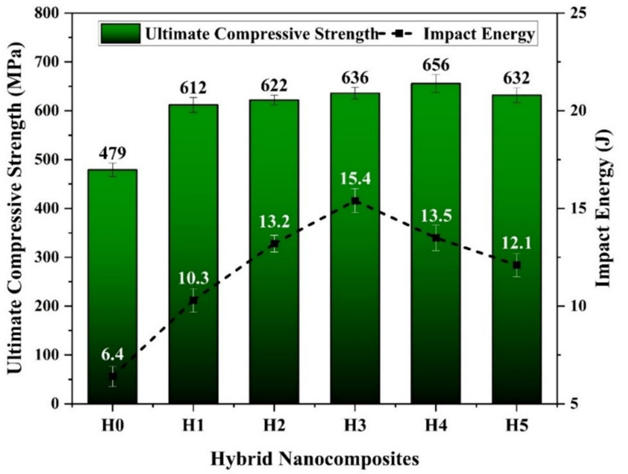

Fig. 13 Ultimate compressive strength and impact energy of LM30+ nB_4C + $nTiO_2$ hybrid nanocomposites

due to the robust interfacial bond and efficient load-bearing effect possessed by both the nano reinforcements that are tightly bound.

3.4.4 Impact Energy Evaluation

The influence of B_4C and TiO_2 nanoparticles on the impact strength of the as-cast LM30 alloy and hybrid nanocomposites are shown in Fig. 13. The toughness or impact energy of a material is often determined by the amount of energy required to cause the material to fracture. The fracture toughness in HAMNC is elevated due to the significant plastic deformation energy present in the stress concentration location [31]. The incorporation of $nTiO_2$ particles increased the impact energy of the hybrid nanocomposites. B_4C and TiO_2 particles at localized stress regions might have hindered the crack propagation by absorbing and releasing the energy during deformation under impact loads. Also, the nanoparticles surrounding the primary silicon, evident from the microstructure study Fig. 4(e), promoted better bonding between the matrix and reinforcement. It increased the energy absorption behavior of the hybrid nanocomposites. The LM30 + nB_4C composite with 0.5 wt. $nTiO_2$ showed impressive resiliency, absorbing (15.4 J) more impact energy than the monolithic LM30 alloy (6.4 J). Beyond 0.5 wt.% of $nTiO_2$ addition, the fracture toughness behavior started to deteriorate. The increased presence of ceramic particles inside the soft matrix might have reduced its ability to withstand plastic deformation [32].

The findings that aided in the enhancement of the mechanical behavior of the processed hybrid nanocomposites may be ascribed to many aspects, namely: (1) the enhancement of proeutectic silicon's quality; (2) the establishment of an effective interfacial bond; (3) the impeding of dislocation motion; and (4) The thermal mismatch between the alloy and the nanoparticles.

4 Conclusion

Hybrid Aluminium Metal Matrix Nanocomposites (HAMNCs) by reinforcing B_4C and TiO_2 nanoparticles with LM30 matrix were made using ultrasonic vibration squeeze-assisted stir-casting. The following observations were made from the various characterization and mechanical tests.

(i) The addition of dual nano ceramic reinforcements aided in refining Si size. Adding up to 0.75 wt.% of $nTiO_2$ to the LM30 + 1 wt.% nB_4C formulations exhibited increased experimental density and reduced porosity. However, further inclusion of $nTiO_2$ increased the porosity level.

(ii) The XRD spectrum analysis highlighted the intensity peaks of TiO_2 and B_4C, confirming the addition of reinforcements to the base matrix. Also, it revealed several elements and compounds such as Al, Si, Al_2Si, Cu_2Al, Al_2CuMg, Mg_2Cu, and $Al_4Ti_2SiO_{12}$.

(iii) The hybrid nanocomposite with 0.75 wt.% $nTiO_2$ (H4) is found to have an increased hardness (107.2 HRB), Ultimate Tensile Strength (256.52 MPa), Ultimate Compressive Strength (656 MPa) due to ultrasonic degassing effect, low porosity by squeeze casting and increased interfacial bonding between matrix and dual nanoparticles. The FESEM revealed the fracture features of the fractured tensile test specimens.

(iv) The LM30 + nB_4C nanocomposite containing 0.5 wt. $nTiO_2$ exhibited remarkable resilience, absorbing fracture toughness to a maximum value of 15.4 J under impact load.

Acknowledgements The authors thank the management and administration of the Vellore Institute of Technology for providing the research infrastructure, support and cooperation for carrying out this research work.

Author Contributions D.K.P.K. designed the concept, interpreted the data and wrote the manuscript. D.G.S edited the manuscript. Both authors reviewed the manuscript.

Funding The authors declare that no funds, grants, or other support were received during the preparation of this manuscript.

Data Availability No datasets were generated or analysed during the current study.

Declarations

Ethics Approval Not applicable.

Consent to Participate Not applicable.

Consent for Publication Not applicable.

Competing Interests The authors declare no competing interests.

References

1. Ramanathan A, Krishnan PK, Muraliraja R (2019) A review on the production of metal matrix composites through stir casting – Furnace design, properties, challenges, and research opportunities. J Manuf Process 42:213–245. https://doi.org/10.1016/j.jmapro.2019.04.017
2. Dinesh Kumar PK, Darius Gnanaraj S (2023) Aluminium-Silicon based Metal Matrix Composites for brake rotor applications: a review. Eng Res Express 5. https://doi.org/10.1088/2631-8695/accdb6
3. Singhal V, Pandey OP (2022) Influence of Dual Range Particle Size on Wear and Friction Properties of Ilmenite Reinforced Aluminium Metal Matrix Composite. Silicon 14:11805–11820. https://doi.org/10.1007/s12633-022-01901-6
4. Sharma M, Singhal V, Gupta A et al (2023) Microstructural, Mechanical and Wear Characteristics of Industrial Waste (Brass Slag) Reinforced LM30 Alloy-Based Composite. Silicon. https://doi.org/10.1007/s12633-023-02665-3
5. Sharma S, Gupta R, Nanda T, Pandey OP (2021) Influence of two different range of sillimanite particle reinforcement on tribological characteristics of LM30 based composites under elevated temperature conditions. Mater Chem Phys 258:123988. https://doi.org/10.1016/j.matchemphys.2020.123988
6. Miladinović S, Stojanović B, Gajević S, Vencl A (2022) Hypereutectic Aluminum Alloys and Composites: A Review. Silicon 2507–2527. https://doi.org/10.1007/s12633-022-02216-2
7. Samal P, Vundavilli PR, Meher A, Mahapatra MM (2020) Recent progress in aluminum metal matrix composites: A review on processing, mechanical and wear properties. J Manuf Process 59:131–152. https://doi.org/10.1016/j.jmapro.2020.09.010
8. Jayaprakash D, Niranjan K, Vinod B (2023) Studies on Mechanical and Microstructural Properties of Aluminium Hybrid Composites: Influence of SiC/Gr Particles by Double Stir-Casting Approach. Silicon 15:1247–1261. https://doi.org/10.1007/s12633-022-02106-7
9. Rajeev VR, Dwivedi DK, Jain SC (2010) Effect of load and reciprocating velocity on the transition from mild to severe wear behavior of Al-Si-SiCp composites in reciprocating conditions. Mater Des 31:4951–4959. https://doi.org/10.1016/j.matdes.2010.05.010
10. Gnaneswaran P, Hariharan V, Chelladurai SJS et al (2022) Investigation on Mechanical and Wear Behaviors of LM6 Aluminium Alloy-Based Hybrid Metal Matrix Composites Using Stir Casting Process. Adv Mater Sci Eng 2022. https://doi.org/10.1155/2022/4116843
11. Madhukar P, Mishra V, Selvaraj N et al (2022) Influence of Ultrasonic Vibration towards the Microstructure Refinement and Particulate Distribution of AA7150-B4C Nanocomposites. Coatings 12. https://doi.org/10.3390/coatings12030365
12. Hu K, Yuan D, Lu S, Wu S (2018) Effects of nano-SiCp content on microstructure and mechanical properties of SiCp/A356 composites assisted with ultrasonic treatment. Trans Nonferrous Met Soc China English Ed 28:2173–2180. https://doi.org/10.1016/S1003-6326(18)64862-9
13. Madhukar P, Selvaraj N, Gujjala R, Rao CSP (2019) Production of high performance AA7150-1% SiC nanocomposite by novel fabrication process of ultrasonication assisted stir casting. Ultrason Sonochem 58:104665. https://doi.org/10.1016/j.ultsonch.2019.104665
14. Yuan D, Yang X, Wu S et al (2019) Development of high strength and toughness nano-SiCp/A356 composites with ultrasonic vibration and squeeze casting. J Mater Process Technol 269:1–9. https://doi.org/10.1016/j.jmatprotec.2019.01.021
15. Pragathi PRE (2023) Mechanical and microstructure behaviour of aluminum nanocomposite fabricated by squeeze casting and ultrasonic aided squeeze casting: A comparative study. J Alloys Compd 956:170203. https://doi.org/10.1016/j.jallcom.2023.170203
16. Harichandran R, Selvakumar N (2018) Microstructure and mechanical characterization of (B4C+ h-BN)/Al hybrid nanocomposites processed by ultrasound assisted casting. Int J Mech Sci 144:814–826. https://doi.org/10.1016/j.ijmecsci.2017.08.039
17. Kannan C, Ramanujam R (2017) Comparative study on the mechanical and microstructural characterisation of AA 7075 nano and hybrid nanocomposites produced by stir and squeeze casting. J Adv Res 8:309–319. https://doi.org/10.1016/j.jare.2017.02.005
18. Shayan M, Eghbali B, Niroumand B (2019) Synthesis of AA2024-(SiO2np+TiO2np) hybrid nanocomposite via stir casting process. Mater Sci Eng A 756:484–491. https://doi.org/10.1016/j.msea.2019.04.089
19. Bharathi P, Sampath Kumar T (2023) Effect of Silicon Carbide and Boron Carbide on Mechanical and Tribological Properties of Aluminium 7075 Composites for Automobile Applications. Silicon 15:6147–6171. https://doi.org/10.1007/s12633-023-02498-0
20. Dinesh Kumar PK, Solomon DG (2023) Investigations on microstructure and mechanical properties on LM30-B4C nanocomposites fabricated through ultrasonic-squeeze assisted stir-casting. Mater Today Commun 37. https://doi.org/10.1016/j.mtcomm.2023.106978
21. Prabhu SR, Shettigar AK, Herbert MA, Rao SS (2019) Microstructure and mechanical properties of rutile-reinforced AA6061 matrix composites produced via stir casting process. Trans Nonferrous Met Soc China English Ed 29:2229–2236. https://doi.org/10.1016/S1003-6326(19)65152-6
22 Shayan M, Eghbali B, Niroumand B (2020) Fabrication of AA2024−TiO2 nanocomposites through stir casting process. Trans Nonferrous Met Soc China English Ed 30:2891–2903. https://doi.org/10.1016/S1003-6326(20)65429-2
23. Madhukar P, Selvaraj N, Rao CSP, Veeresh Kumar GB (2019) Tribological behavior of ultrasonic assisted double stir casted novel nano-composite material (AA7150-hBN) using Taguchi technique. Compos Part B Eng 175. https://doi.org/10.1016/j.compositesb.2019.107136
24. Mann VS, Pandey OP (2021) Effect of Dual Particle Size Corundum Particles on the Tribological Properties of LM30 Aluminium Alloy Composites for Brake Rotor Applications. Arab J Sci Eng 46:12445–12463. https://doi.org/10.1007/s13369-021-05939-3
25. Abdudeen A, Mourad AHI, Qudeiri JA, Ziout A (2020) Evaluation of characteristics of A390 - SiCp squeeze cast and gravity cast composites. 2020 Adv Sci Eng Technol Int Conf ASET 2020. https://doi.org/10.1109/ASET48392.2020.9118349
26. Dinesh Kumar PK, Darius Gnanaraj S (2024) Studies on Al-Si based hybrid aluminium metal matrix nanocomposites. Mater Today Commun 38. https://doi.org/10.1016/j.mtcomm.2024.108132
27. Arivukkarasan S, Dhanalakshmi V, Stalin B, Ravichandran M (2018) Mechanical and tribological behaviour of tungsten carbide reinforced aluminum LM4 matrix composites. Part Sci Technol 36:967–973. https://doi.org/10.1080/02726351.2017.1331285
28. Madhukar P, Selvaraj N, Rao CSP, Kumar GBV (2020) Enhanced performance of AA7150-SiC nanocomposites synthesized by novel fabrication process. 46:17103–17111. https://doi.org/10.1016/j.ceramint.2020.04.007

29. Pragathi P, Elansezhian R (2022) Studies on microstructural and mechanical properties of (Nano SiC + Waste Spent catalyst) reinforced aluminum matrix composites. Mater Today Commun 30:103204. https://doi.org/10.1016/j.mtcomm.2022.103204
30. Tharanikumar L, Mohan B, Anbuchezhiyan G (2022) Enhancing the microstructure and mechanical properties of Si3N4-BN strengthened Al-Zn-Mg alloy hybrid nano composites using vacuum assisted stir casting method. J Mater Res Technol 20:3646–3655. https://doi.org/10.1016/j.jmrt.2022.08.093
31. Ozden S, Ekici R, Nair F (2007) Investigation of impact behaviour of aluminium based SiC particle reinforced metal-matrix composites. Compos Part A Appl Sci Manuf 38:484–494. https://doi.org/10.1016/j.compositesa.2006.02.026
32. Reddy PS, Kesavan R, Vijaya Ramnath B (2018) Investigation of Mechanical Properties of Aluminium 6061-Silicon Carbide, Boron Carbide Metal Matrix Composite. Silicon 10:495–502. https://doi.org/10.1007/s12633-016-9479-8

Publisher's Note Springer Nature remains neutral with regard to jurisdictional claims in published maps and institutional affiliations.